Research Article

Amira Ben Gouider Trabelsi, Fatemah H. Alkallas, Mohamed S. I. Koubisy, Wael M. Mohammed, Mahmoud M. Abou Halaka, and Abdelaziz M. Aboraia*

Unveiling the transformative role of samarium in ZnO: Exploring structural and optical modifications for advanced functional applications

https://doi.org/10.1515/phys-2025-0205
received April 30, 2025; accepted June 27, 2025

Abstract: The current study investigates the optical characteristics of $Zn_{100-x}Sm_xO$ thin films, focusing on the effects of Samarium (Sm) doping on absorbance, transmittance, and nonlinear optical properties. Thin films were synthesized with varying Sm concentrations using a solid-state synthesis method. UV-Vis spectroscopy revealed a gradual decrease in the optical band gap, with the highest value of 3.12 eV for $x = 0$ and 2.76 eV for $x = 10$, indicating improved light absorption capabilities with increasing Sm content. The nonlinear absorption coefficient of the Sm ratio shifted from 18.7 to 23 cm/GW for $x = 0$ and 10, respectively, which is attributed to the introduction of new energy levels within the band gap, facilitating electron transitions. The lattice dielectric constant (ε_1) of the Sm ratio increased from 1.43 to 2.1 for $x = 0$ and 10, respectively, revealing enhanced polarization. Additionally, the calculated values of the static refractive index were found to increase from 1.13 for $x = 0$ to 1.33 for $x = 10$, supporting the observed behavior of ε_1. These findings provide valuable insights into the tunable optical properties of $Zn_{100-x}Sm_xO$ thin films, highlighting their promising applications in optoelectronic devices. This study opens avenues for the continued refinement of $Zn_{100-x}Sm_xO$ and related materials, enhancing their suitability for a range of technological uses.

Keywords: refractive index, optical properties, thin films, nonlinear optical effect

1 Introduction

Nanocomposites play a pivotal role in advancing materials science, as highlighted by recent studies [1–3]. They exhibit enhanced photocatalytic properties for environmental protection, effectively degrading organic pollutants and enabling applications in antibacterial surfaces and self-cleaning materials, as noted in one study. Another research emphasizes their efficiency in wastewater treatment, utilizing PSA-based nanocomposites for adsorption and photocatalysis to remove heavy metals and antibiotics. Additionally, polymer nanocomposites improve mechanical and optical properties, supporting diverse applications in industrial, domestic, and biomedical fields, underscoring their versatility and significance.

ZnO stands out as an important material because its properties consist of the broad bandgap energy and strong exciton binding energy (~3.37 eV and ~60 meV, respectively) while demonstrating strong chemical stability. ZnO demonstrates desirable characteristics that enable its implementation in various optoelectronic and photovoltaic devices and sensor and photocatalyst technologies [4–7]. The structural and optical features of ZnO films become more adaptable by the addition of rare-earth elements. Among dopants, samarium (Sm) from the lanthanide group is unique due to its capability to produce localized energy levels within the ZnO bandgap, which results in improved luminescence functionality and modified electronic characteristics [8]. Also, zinc oxide (ZnO) exhibits exceptional properties, including a wide bandgap (~3.37 eV), high exciton binding energy (60 meV), and strong room-temperature luminescence. Doping ZnO

* **Corresponding author: Abdelaziz M. Aboraia**, Department of Physics, Faculty of Science, Al-Azhar University, Assiut, Egypt, e-mail: a.m.aboraia@gmail.com, a.m.aboraia@azhar.edu.eg
Amira Ben Gouider Trabelsi, Fatemah H. Alkallas: Department of Physics, College of Science, Princess Nourah Bint Abdulrahman University, P.O. Box 84428, Riyadh, 11671, Saudi Arabia
Mohamed S. I. Koubisy: Department of Physics, Faculty of Science, Al-Azhar University, Assiut, Egypt
Wael M. Mohammed: Physics Department, Faculty of Science, Minia University, P.O. Box 61519, Minia, Egypt
Mahmoud M. Abou Halaka: Department of Radiology, College of Health and Medical Technology, Al-Ayen University, Thi-Qar, 64001, Iraq

with samarium (Sm) introduces 4f electronic states, which can enhance optical absorption, tune bandgap energy, and improve electrical conductivity due to Sm^{3+}/Sm^{2+} redox activity. Sm doping also modifies defect-related emissions, making it promising for optoelectronic and photocatalytic applications [8].

ZnO thin film materials experiencing rare-earth doping have received extensive research to enhance their operational capacity for innovative technological developments. Visible-spectrum photoluminescence releases emerge from the precise intra-4f transition behavior of samarium [9]. The addition of Sm atoms to the ZnO material led to some changes in both optical propagation and structural dimensions, including phases and granule features. Research on Sm-doped ZnO thin films needs additional systematic studies regarding structural and optical property evaluation to achieve optimal device performance in optoelectronic applications [10,11].

This study consists of analyzing Sm-doped ZnO thin-film synthesis, followed by their structural and optical measurement process to examine Sm doping effects on material properties. Our goal is to understand the relationship between Sm concentration and the outcome properties of thin films through advanced characterization methods. During the last several decades, research on ZnO-based materials has maintained its status as a central research priority [12]. The crystal structure of pure ZnO matches that of wurtzite, while it enables high visibility in the visible spectrum, thus becoming suitable for light-emitting diodes (LEDs) and transparent conducting oxides (TCOs). Researchers oversee pure ZnO deficiencies because it shows restricted electrical conductivity and below-average emission performances, leading scientists to investigate doping procedures for improved characteristics [13,14].

Scientific investigations into rare-earth elements in ZnO have become more prevalent because these elements introduce exceptional fundamental optical and electronic properties to the material. Scientists have established that europium (Eu), erbium (Er), and neodymium (Nd) dopants increase luminescence outputs while simultaneously improving electrical conductivity and altering bandgap characteristics [15,16]. Sm adds characteristic optical behavior to the visible spectrum through its 4f shell structure, which partially occupies electrons. By introducing samarium doping to ZnO, the substance becomes an appealing material for display technologies and bioimaging applications and solid-state lighting [9].

Different approaches have been documented in previous research regarding Sm-doped ZnO thin film synthesis, which can be achieved through chemical vapor deposition (CVD), sol–gel processing, pulsed laser deposition (PLD), and plasma-assisted sputtering. Research using X-ray diffraction (XRD) showed that Sm doping causes both structural lattice distortions and decreases the crystallite size because Sm^{3+} and Zn^{2+} have different ionic radii [9]. The absorption edge undergoes redshift while photoluminescence intensity increases with increasing Sm doping levels because defect states and intra-4f Sm^{3+} transitions occur according to optical tests [17,18].

The existing research shows progress, but various knowledge gaps exist within the obtained literature. For example:

1) Scientists are still discussing the most effective amount of Sm doping needed to maximize optical property improvements.
2) The link between structural modifications and optical responses in ZnO crystals must be fully analyzed.
3) A thorough examination of Sm-doped ZnO thin film properties during synthesis requires investigation of synthesis parameters, including the annealing temperature and precursor concentration.

The main goal of this study is to investigate the optical and structural characteristics of Sm-doped ZnO thin films created using a controlled deposition method.

2 Experimental methods

All chemical substances, such as isopropanol, citric acetate, samarium oxide, and zinc nitrate, were obtained from Sigma Aldrich. The synthesis of $Zn_{100-x}Sm_xO$ nanoparticles with x values from 0 to 10 and 2.5 to 10 was performed using the sol–gel combustion technique. The synthesis required 50 mL of isopropanol, which fully dissolved zinc nitrate with samarium oxide, along with citric acid in a beaker. The mixing operation occurred at normal temperature as researchers maintained equal ratios between citric acid and metal cations. A magnetic stirrer was used to heat the mixture to 150°C, and a gel was formed after the evaporation was completed with persistent stirring. The material was ignited when heated again, which produced an abundant flaming substance. The product was exposed to heat at 600°C before being ground into small particles. The gel-combustion method is considered the preferred approach in laboratories because it offers easy execution together with low costs, and maximum efficiency. This method follows circular economy principles because it combines sustainable reuse of resources with its resource-efficient characteristics [19–21]. The method implements the circular economy principles through its combination of sustainable resource reusability and resource utilization efficiency. The films were

formed by mixing ZnO:Sm powder with chitosan solution at their optimal concentration level. The drying process required the application of optimized parameters for film application onto substrates to achieve uniformity and optimal performance. The films were deposited using solutions created by combining ZnO:Sm powder with chitosan solution at an appropriate concentration. During the drying process, the films were coated onto the substrate using optimized dip-coating parameters. A few drops (typically ~50–100 µL) of the prepared ZnO precursor solution were dropped or dispensed onto the center of the substrate. The most effective conditions involved dip-coating for 1 h at a withdrawal speed

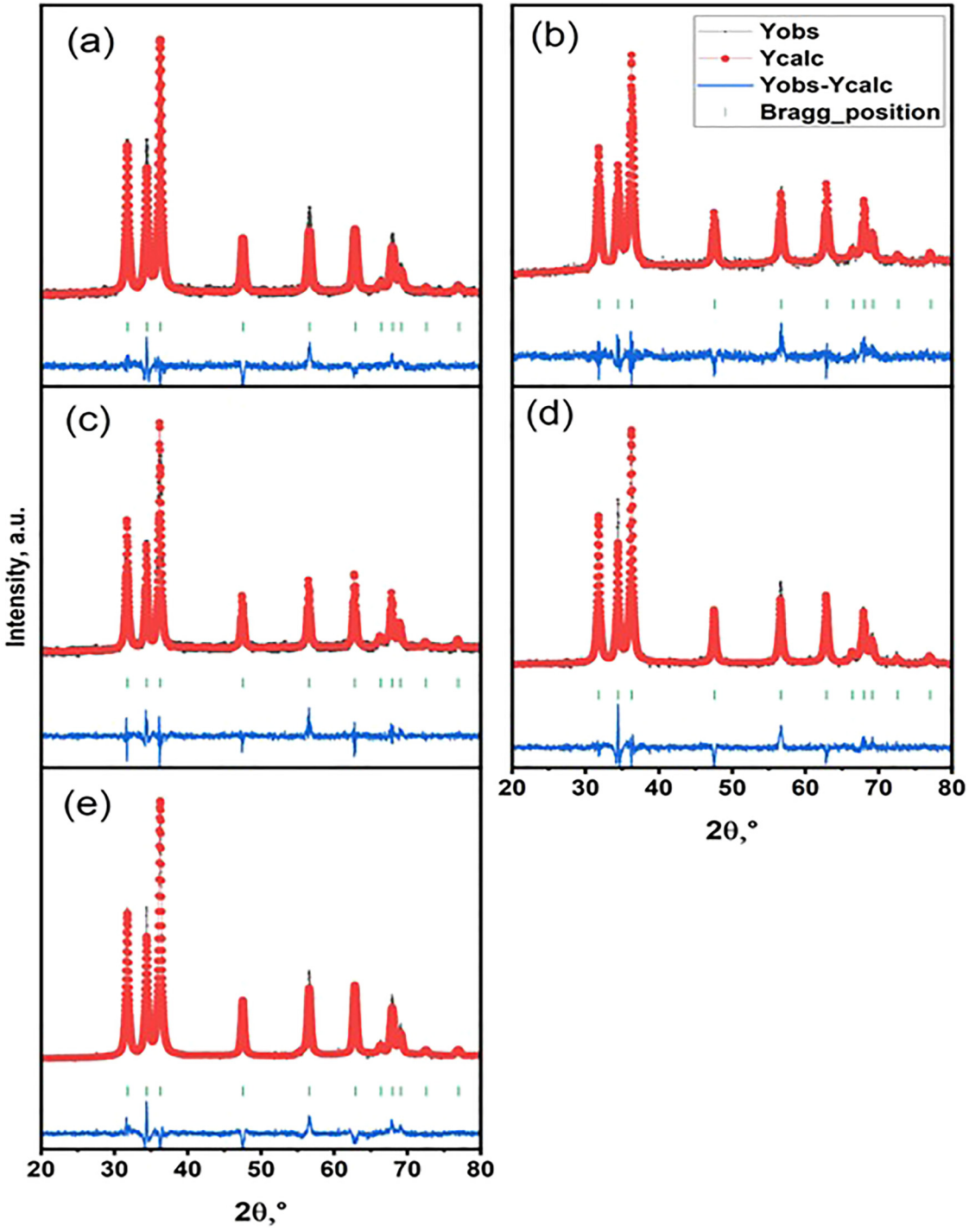

Figure 1: The XRD patterns of (a) ZnO, (b) $Zn_{97.5}Sm_{2.5}O$, (c) Zn_{95} Sm_5O, (d) $Zn_{92.5}Sm_{7.5}O$, and (e) $Zn_{90}Sm_{10}O$.

Table 1: Calculated lattice parameters of ZnO, $Zn_{97.5}Sm_{2.5}O$, Zn_{95} Sm_5O, $Zn_{92.5}Sm_{7.5}O$, and $Zn_{90}Sm_{10}O$

Thin film	$a = b$ (Å)	c (Å)	V (Å^3)
ZnO	3.248	5.209	47.612
$Zn_{97.5}Sm_{2.5}O$	3.251	5.211	47.712
Zn_{95} Sm_5O	3.252	5.212	47.738
$Zn_{92.5}Sm_{7.5}O$	3.253	5.213	47.785
$Zn_{90}Sm_{10}O$	3.256	5.217	47.913

of 40 mm/min. Following deposition, the films were annealed at 300°C in a nitrogen atmosphere, with a controlled heating rate of 0.2°C/min. The crystal structures of pure ZnO and ZnO:Sm powders were studied using a LAScientific XRD with CuKα radiation (λ = 1.54 Å). Field emission scanning electron microscopy (FE-SEM) was carried out using a Supra (Ziess) scanning electron microscope, which was operated at 15.0 kV. Jasco V670 was used to investigate both the optical bandgap and transmission spectra of the current samples.

3 Results and discussion

The XRD patterns of $Zn_{100-x}Sm_xO$ (ZnO:Sm) solid-state produced powders with x = 0.0, 2.50, 5.0, 7.50, and 10.0 are shown in Figure 1(a)–(e). The measurement data from X-ray diffraction (XRD) presented well-defined peaks, indicating the hexagonal wurtzite structure of ZnO, which exists as the $P6_3mc$ space group, to demonstrate the crystalline behavior of all ZnO:Sm samples. The diminished intensity of ZnO:Sm samples of the (002) diffraction peak signifies decreased growth rate along with limited crystallization. The wurtzite ZnO peaks of each composition demonstrate the (101) reflection plane orientation as their preferred structure. Peak position analysis was used by the Standard Joint Committee for Powder Diffraction Standards reference (JCPDS card no. 01-080-0075) to confirm the material's polycrystalline structure [21,22]. The lattice parameters were decreased at low Sm concentrations because Zn^{2+} ions were replaced by Sm^{3+} ions in the crystal structure. Similar changes were observed for ZnO materials containing dopants such as Er, Sm, and Ce. This parameter change occurs when Sm^{3+} with its 0.964 nm radius replaces Zn^{2+} with a 0.74 nm radius. A minor peak displacement toward elevated 2θ values supports the ion substitution process. Further increases in Sm doping levels lead to a shift in the trend due to increasing defect densities resulting from substitutional doping. The synthesis pressure and temperature, along with impurity atoms and defects, as well as the difference in the ionic radii between Zn^{2+} and Sm^{3+} influence the ZnO crystal lattice parameters a and c. When Zn^{2+} ions are replaced by Sm^{3+} ions in ZnO, there is a reduction in the peak intensity along with lattice parameter modification, which jointly creates structural strain and distorts the crystal lattice, as exhibited in Table 1.

Scanning electron microscopy (SEM) images of pure ZnO and ZnO:Sm thin films with varying Sm concentrations are presented in Figure 2. The micrographs reveal distinct grain boundaries, with grain sizes decreasing as Sm content increases. This reduction is attributed to the incorporation of Sm^{3+} ions, which inhibit grain growth by exerting an interaction force at grain boundaries, altering the nucleation and growth kinetics. The crystallite size and

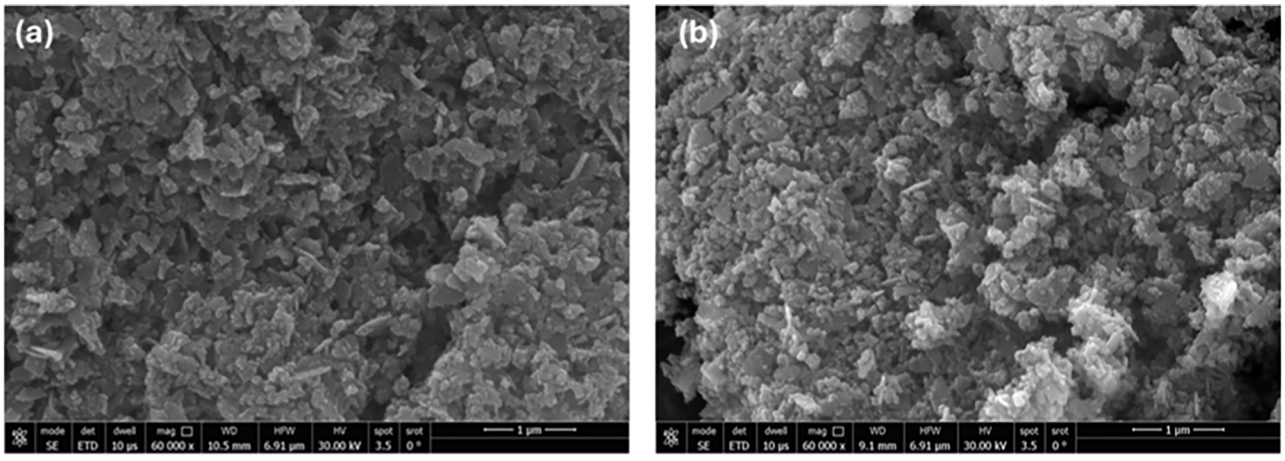

Figure 2: The SEM photo of (a) pure ZnO and (b) $Zn_{90}Sm_{10}O$.

microstructure are influenced by the dopant type and ionic radius of Sm^{3+} (approximately 0.96 Å), which differs from that of Zn^{2+} (0.74 Å), inducing lattice strain and limiting grain expansion. The SEM images also highlight well-defined pores, whose size and density correlate inversely with Sm concentration. As Sm content increases, the pore size decreases, reflecting enhanced surface densification due to improved particle packing. Higher Sm doping levels increase surface roughness and compactness, indicative of better particle densification and reduced porosity, which can enhance mechanical stability and optical properties.

Figure 3 shows the roughness of Sm-doped ZnO thin films, as described by the RMS (root mean square roughness) values for different Sm concentrations, which reveals a non-linear trend with increasing doping. The structured analysis is shown in Table 2. The RMS roughness of 0.484 nm for undoped ZnO indicates an atomically flat surface, typical of well-deposited thin films. This serves as a reference for evaluating the doping effects. At 2.5% Sm ($Zn_{0.975}Sm_{0.025}O$), the RMS increases to 8.52 µm, suggesting that Sm incorporation disrupts the ZnO lattice, leading to surface irregularities. The possible causes are lattice strain, localized clustering of Sm ions, or nucleation of secondary phases. At 5% Sm ($Zn_{0.95}Sm_{0.05}O$), the RMS increases to 15.07 µm, the roughest film. This implies severe surface degradation, likely due to excessive Sm ions segregating to grain boundaries or forming Sm-rich clusters, and

Table 2: Roughness and RMS of $Zn_{100-x}Sm_xO$ (x = 0, 0.025, 0.05, and 0.075)

Sample $Zn_{100-x}Sm_xO$	Roughness × 10^{-6}	RMS of roughness × 10^{-6}
X = 0	484.015 × 10^{-3}	761.65 × 10^{-3}
X = 2.5	8.52	12.59
X = 5	15.07	18.58
X = 7.5	8.010	10.22

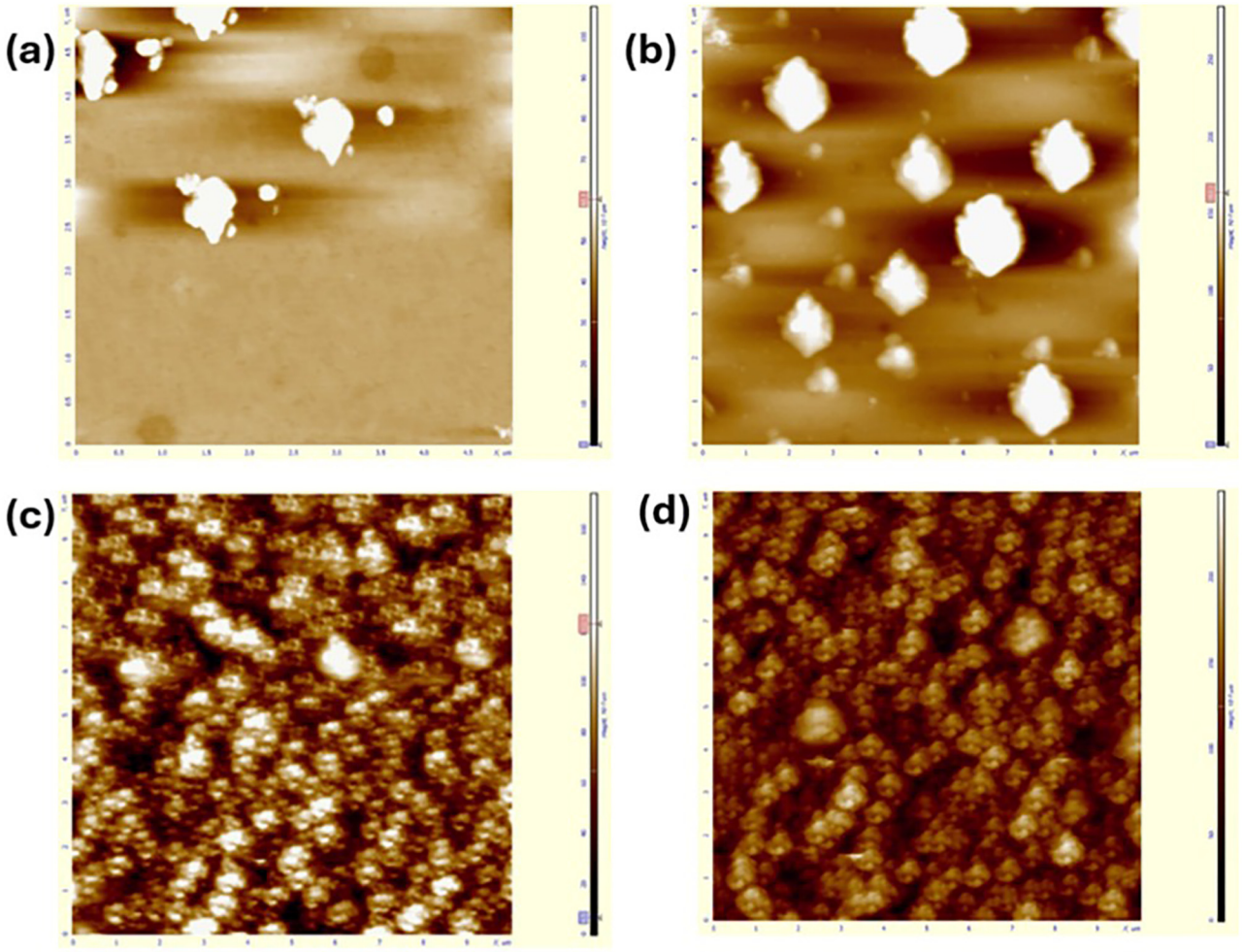

Figure 3: (a)–(d) AFM photos of $Zn_{100-x}Sm_xO$ (x = 0, 0.025, 0.05, and 0.075).

enhanced grain growth or agglomeration during deposition. At 7.5% Sm ($Zn_{0.925}Sm_{0.075}O$), the RMS decreases to 8.01 µm, indicating partial recovery of surface smoothness. This could arise from the saturation of defect/clustering effects, reorganization of the film microstructure (*e.g.*, larger, smoother grains dominating the surface), and the formation of a stable Sm–Zn–O ternary phase that mitigates roughness.

4 Implications for applications

Optoelectronics: High roughness (*e.g.*, 15.07 nm at 5% Sm) could scatter light or degrade device interfaces, reducing efficiency. Sensors/catalysts: Increased surface area from roughness might enhance reactivity, but excessive roughness could destabilize device performance. Mechanical stability: Films with high RMS roughness may suffer reduced adhesion or mechanical integrity.

The relationship between a material's absorbance and wavelength can reveal information about its electronic structure. The spectral peaks that correspond to electronic transitions, however, help clarify molecular activity and effects [23,24]. The dependencies of the absorbance on the wavelength of the $Zn_{100-x}Sm_xO$ pure thin film (x = 0) and those thin films doped with different concentrations of samarium (x = 2.5, 5, 7.5, and 10) are exhibited in Figure 4. The increase in the Sm concentration led to an increase in the absorbance of the thin films. This suggests that the addition of Sm enhances the material's ability to absorb light at the measured wavelengths. This might be the result of new electronic states entering the material's bandgap, which allows for greater light absorption [25]. Also, it is observed that the absorbance peaks' amplitude increases with Sm concentration, suggesting that transitions associated with these peaks are either more likely to be strong or more strong. The substitution of Sm with Zn may have caused more traps or defects to form in the crystal lattice, which may have facilitated electronic transitions [26]. The electrical structure of the ZnO lattice may change if Sm is added. Since Sm is a rare earth element, it may change the valence and conduction bands or introduce localized states, which would improve the absorption properties. If the bandgap narrows, it may also cause the absorption spectra to red shift. Higher Sm concentrations may improve the material's photocatalytic qualities, enhancing its usefulness for processes like photocatalysis or solar energy harvesting, according to the increased absorbance in the visible spectrum.

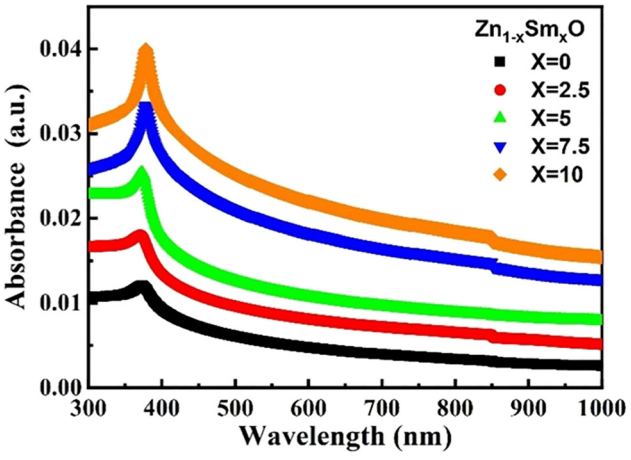

Figure 4: Wavelength dependence of the absorbance for the $Zn_{100-x}Sm_xO$ thin films.

Understanding and constructing optical devices requires an understanding of thin film transmittance and reflectance. Reflectance reveals how much light is reflected from the film, whereas transmittance shows how much light flows through it. These characteristics, which allow for modifications to control the interaction of light with the film at particular wavelengths, are strongly dependent on the thickness and material composition of the film. Figure 5a and b shows the dependency of the transmittance and reflectance, respectively, on the wavelength. In the case of transmittance (Figure 5a), increasing the amount of Sm in the material reduces how much of light that passes through it. This is probably because Sm is causing the material to absorb or scatter more light. The presence of Sm likely introduces new energy levels or imperfections in the ZnO structure, which leads to greater light absorption and, consequently, less light transmission [27]. As Sm is introduced, certain electronic transitions appear to become more prominent, as seen by the observed peaks' increased amplitude with larger Sm ratios. This might be because higher absorption peaks result from the creation of localized states that increase the probability of transitions. As for the reflectance (Figure 5b), it increases with increasing Sm concentration. This can be attributed to changes in the refractive index of the material due to doping. Greater Sm concentrations may cause more scattering at internal or external surfaces, which would cause more light to be reflected rather than transmitted [28]. According to the changes in optical characteristics, the current thin films may be customized for certain applications, such as photocatalytic systems where light control is critical or optoelectronic devices where regulated absorption and reflection are critical.

The absorption coefficient (α) of any material can help in identifying and understanding the material's composition and structure. Therefore, this is essential for designing optical devices like solar cells, lenses, and filters. The

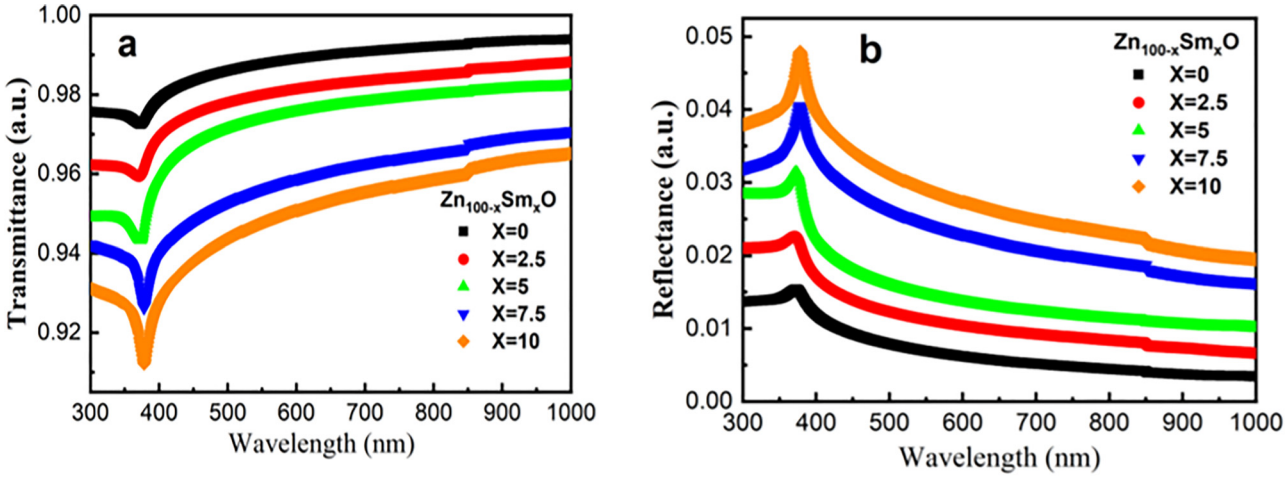

Figure 5: (a) Transmittance and (b) reflectance as a function of wavelength for the $Zn_{100-x}Sm_xO$ thin films.

absorption coefficient can be estimated *via* the transmittance (T) and reflectance (R) as follows [27,29,30]:

$$\alpha = \frac{1}{d}\ln\left[\frac{(1-R)^2 + [(1-R)^4 + 4R^2T^2]^{1/2}}{2T}\right], \quad (1)$$

where d represents the film thickness. Figure 6 demonstrates the change of α through photon energy. α is observed to increase with increasing Sm ratio, suggesting that doping with Sm improves the material's absorption of light, most likely because it creates new energy levels in the bandgap that make electrical transitions easier. Also, the absorption coefficient increases with the photon energy, which is typical for semiconductor materials. The sharp peak observed in Figure 6 indicates resonant transitions; this peak slightly increases as the Sm ratio increases (from $x = 0$ to $x = 10$), suggesting that a higher density of accessible electronic states at higher Sm concentrations increases the probability of photon absorption at such energies. The shifting and broadening of the peaks as the Sm concentration increases can be ascribed to doping-induced changes in the ZnO's electrical structure. One possible explanation for this could be the creation of localized states that change the band structure and hence reduce the energy needed for specific electronic transitions.

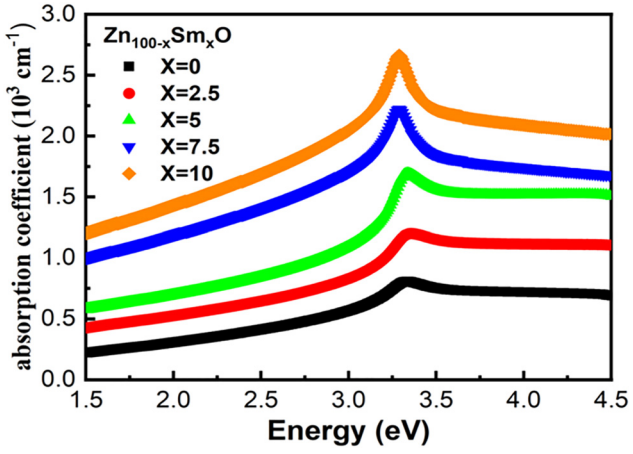

Figure 6: Absorbance coefficient for the $Zn_{100-x}Sm_xO$ thin films.

The Urbach tail, in conjunction with sub-bandgap photon energy, suggests structural instability in thin-film semiconductors. The observation links to states that form locally [31]. The well-known empirical method can be used to determine the Urbach energy in the low photon energy area [32–34], as follows:

$$\alpha(\nu) = \alpha_0 \exp\left(\frac{h\nu}{E_u}\right). \quad (2)$$

The parameters ν, h, α_0, and α stand for the frequency, Planck's constant, a constant, and the absorption coefficient, respectively. Eq. (2) can be written as

$$\ln(\alpha(\nu)) = \ln(\alpha_0) + \frac{1}{E_u}h\nu. \quad (3)$$

Using the slope of the relationship between the photon energy and ln (α) (Figure 7a), the Urbach energy values were determined. The Urbach energy increases as the Sm ratio increases, as exhibited in Figure 7b. This might be explained by the notable changes in the electronic characteristics owing to the increase in the Sm ratio, which can change the band structure and cause the band tail to expand, thereby increasing the Urbach energy. This behavior was seen for S_xWO_3 [32]. This could improve light absorption, which is advantageous for some applications like photovoltaic cells. Additionally, the optical energy gap (E_g^{Opt}) for $Zn_{100-x}Sm_xO$ thin films at the high absorption edge was calculated using the Tauc formula [34] as follows:

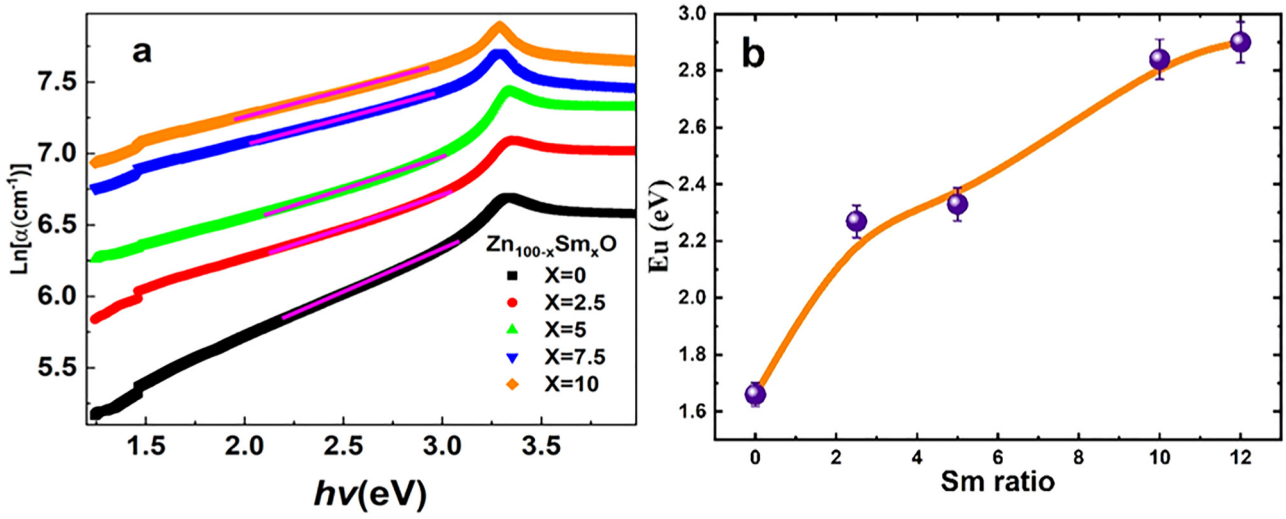

Figure 7: (a) Variation of ln(α) with the photon energy for $Zn_{100-x}Sm_xO$ and (b) urbach energy *vs* Sm concentration.

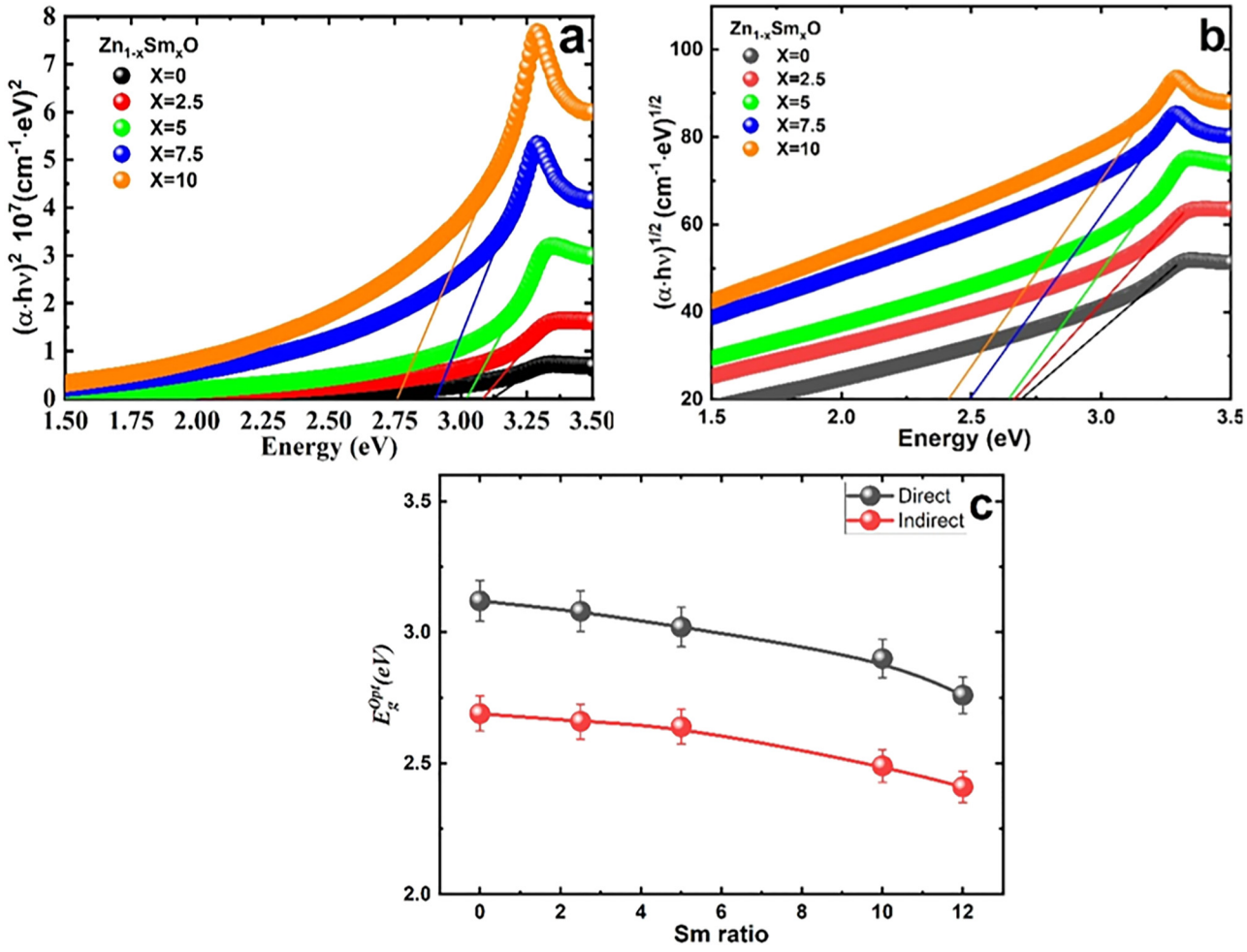

Figure 8: Optical properties of $Zn_{100-x}Sm_xO$ for varying Sm concentrations (x): (a) $(ahv)^2$ plotted against photon energy, (b) $(ahv)^{(1/2)}$ versus photon energy for the same Sm ratios, illustrating the transition between direct and indirect bandgap behavior and (c) energy gap (Eg^{Opt}) as a function of Sm ratio.

$$ahv = B(hv - E_g^{opt})^A, \quad (4)$$

where B is the Tauc parameter and A is a constant control. Optical transitions can be directly or indirectly enabled by semiconductors [35]. The transition energy values were computed by fitting the linear portion observed in the relationship between $(ahv)^{\frac{1}{n}}$ and hv, wherever the intercept with the x-axis represents the transition energy values. A direct or indirect transition is determined by the value of $\left[\frac{1}{n}\right]$. When $\left[\frac{1}{n}\right] = 2$, it indicates a direct transition, and when $1/n = 1/2$, it indicates an indirect transition. The hv dependences of $(ahv)^2$ and $(ahv)^{1/2}$ are plotted in Figure 8a and b, respectively. The data presented in the figure indicate that the linear part of the $(ahv)^2$ plot *versus* (hv) exhibits a clearer and more pronounced linearity compared to the linear region observed in the plot of $(ahv)^{1/2}$ *vs* (hv). This finding implies that a direct electronic transition predominates in the thin films under investigation. Such behaviors were observed in previous studies for TiO_2 nanotube arrays and nanostructured rock wool [36,37]. Figure 8c shows the direct and the indirect energy gap values of the thin films under investigation. The direct E_g^{Opt} values generally decreased when Sm was added to the structure at the expense of Zn; the maximum E_g^{Opt} value (3.12 eV) was achieved for $x = 0$, while the lowest E_g^{Opt} value (2.77 eV) was obtained for $x = 10$ of Sm. The decrease in the direct energy band gap of $Zn_{100-x}Sm_xO$ as the ratio of Sm increases can be related to the differences in the electronic characteristics of Sm compared to Zn. As a result, localized states may be introduced within the band gap. These states can facilitate transitions that lower the effective band gap energy.

The quantity of light that can be absorbed or scattered by any substance is measured by the extinction coefficient (k). The following formula is used to calculate the extinction coefficient:

$$k = \frac{\alpha\lambda}{4\pi}, \quad (5)$$

where α is the absorption coefficient and λ is the wavelength. The wavelength dependency of the extinction coefficient (K) of the $Zn_{100-x}Sm_xO$ thin films is displayed in Figure 9. The fact that K increases as x increases indicates that the addition of Sm to the ZnO matrix improves the material's light-absorbing capacity. The incorporation of Sm ions may cause disruptions in the crystal lattice of ZnO, resulting in defects and localized states that enhance light absorption. Moreover, higher concentrations of Sm introduce more electronic states inside the band gap, which can facilitate electronic transitions and increase absorption. The same behavior was observed for quinoline azo-dye polymers [38].

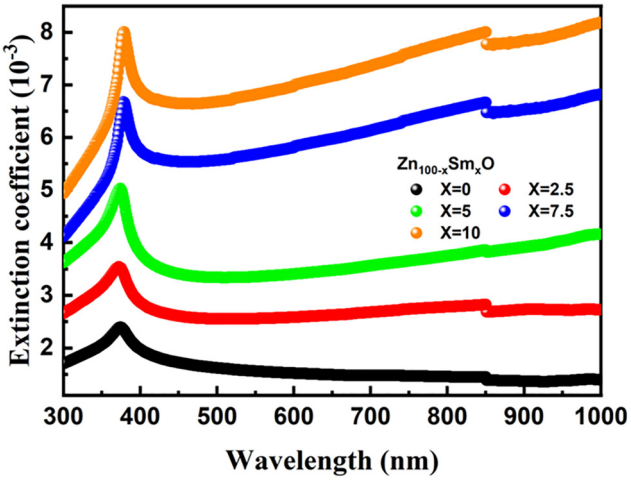

Figure 9: Wavelength dependence of the extinction coefficients for $Zn_{100-x}Sm_xO$ thin films.

To determine the local field and electronic polarization of the atoms or ions in thin-film materials, the refractive index (n) should be examined. A common approach to determine the n value is through the transmittance (T) and reflectance (R) measurements [39]:

$$n = \left(\frac{(1+R)}{(1-R)}\right) + \sqrt{\left(\frac{(1+R)}{(1-R)}\right)^2 - k^2 + 1}. \quad (6)$$

Figure 10a shows the wavelength dependence of the refractive index of the $Zn_{100-x}Sm_xO$ thin films. The increase in the refractive index with increasing Sm is due to changes in the material's electronic and structural characteristics, which improve its optical capabilities. This enhancement could be beneficial for different applications that involve light manipulation and sophisticated optical devices. The measured refractive index values for the thin films under investigation range between 200 and 1,000 nm in wavelength, which is rather close to those obtained using the Cauchy formula [40]. More optical properties have been calculated using the calculated values of the refractive indices. For instance, the dispersion parameters are crucial for enhancing optical communication systems and spectral dispersion control devices. To completely understand the optical characteristics of the films under study, one must have a thorough understanding of the single oscillator energy (E_0) and dispersion energy (E_d). These energies and the energy carried by a photon (hv) are related by the Wemple–DiDomenico model, which is used under these conditions [41]:

$$(n^2 - 1)^{-1} = \frac{E_0^2 - (hv)^2}{E_0E_d} = \frac{E_0}{E_d} - \frac{(hv)^2}{E_0E_d}, \quad (7)$$

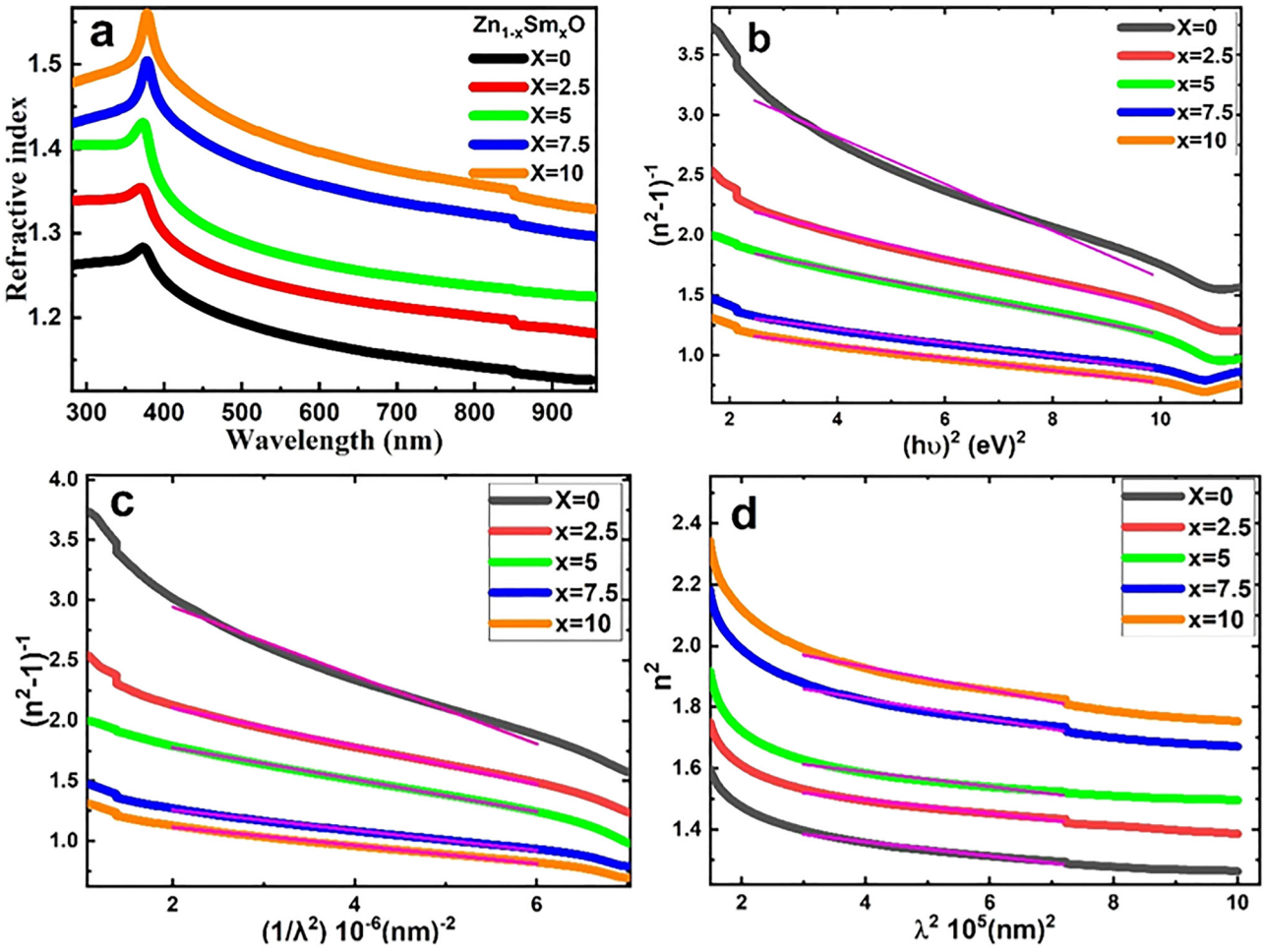

Figure 10: The deduced values involve: (a) refractive index variation with λ, (b) variation of $(n^2 - 1)^{-1}$ with $(h\nu)^2$ to estimate E_0 and E_d, (c) the relation between $(n^2 - 1)^{-1}$ and $(1/\lambda^2)$ for obtaining S_0 and λ_0, and (d) λ^2 dependence of n^2 to calculate εL and N/m* for $Zn_{100-x}Sm_xO$ thin films for different Sm ratios.

or

$$(n^2 - 1)^{-1} = \frac{E_0}{E_d} - \frac{1}{E_0 E_d}(h\nu)^2. \quad (8)$$

Using a graphical representation of $(n^2-1)^{-1}$ *vs* $(h\nu)^2$, E_0 and E_d parameters have been determined (Figure 10b). Table 1 shows the E_0 and E_d values in a structured way. The lattice dielectric constant (ε_∞) and static refractive index (n_0) can be computed using the following formula, which relies on the constants E_0 and E_d [42]:

$$\varepsilon_\infty = \frac{E_d + E_0}{E_0} \text{ and } n_0 = \sqrt{\frac{E_d + E_0}{E_0}}. \quad (9)$$

As observed in Table 3, the values of n_0 and ε_∞ are increased as the ratio of Sm increases. This indicates an enhanced optical density and dielectric polarization for the thin films under investigation by the incorporation of Sm. Also, using the parameters E_0 and E_d, the material's oscillator strength was calculated, where [$f = E_d \times E_0$], and are listed in Table 3.

Table 3: Optical parameter changes of the $Zn_{100-x}Sm_xO$ thin films

Sample $Zn_{100-x}Sm_xO$	Direct E_g^{Opt} (eV)	Indirect E_g^{Opt} (eV)	E_u (eV)	E_d (eV)	E_0 (eV)	F	n_0	ε_∞	$S_0 \times 10^{-6}$ (nm^2)	λ_o (nm)	$N/m^* \times 10^{38}$ (m^{-3} × kg^{-1})	ε_L
$X = 0$	3.12±	2.69	1.66	1.18	4.25	5.02	1.13	1.28	3.52	284.50	2.87	1.43
$X = 2.5$	3.08	2.66	2.27	1.91	4.68	8.94	1.19	1.41	6.35	255.00	2.72	1.58
$X = 5$	3.02	2.64	2.33	2.32	4.80	11.14	1.22	1.48	7.53	255.15	2.95	1.66
$X = 7.5$	2.9	2.49	2.84	3.40	4.90	16.66	1.30	1.69	11.95	242.00	4.03	1.94
$X = 10$	2.76	2.41	2.9	3.95	5.14	20.30	1.33	1.77	13.22	244.00	4.65	2.10

The Sellmeier dispersion model is employed to determine λ_0 (resonance wavelength) and s_0 (oscillator strength) values, particularly at lower frequencies. This is crucial for understanding how light interacts with the material across different wavelengths. The model's effectiveness at lower frequencies suggests its usefulness in analyzing the optical phenomena [43]:

$$\frac{1}{(n^2-1)} = \left(\frac{1}{s_0\lambda_0^2}\right) - \left(\frac{1}{s_0}\cdot\frac{1}{\lambda^2}\right). \tag{10}$$

As exhibited in Figure 10(c), λ_0 and s_0 values can be obtained from the linear fitting of $\frac{1}{(n^2-1)}$ *vs* $\left(\frac{1}{\lambda^2}\right)$, and are listed in Table 3. ε_L (lattice dielectric constant) describes the degree of the responsibility of the material to the applied electrical field at low frequencies or the capacity of the substance to store electrical energy as polarization [44,45]. The term (N/m^*) represents the charge carrier contribution to the refractive index, indicating that the material's refractive index will change when the density of charge carriers increases or their effective mass decreases. Therefore, it is important to measure these two parameters $\left(\varepsilon_L \text{ and } \frac{N}{m^*}\right)$ for the investigated thin films. Figure 10(d) exhibits the relationship between n^2 and λ^2, and the parameters ε_L and $\frac{N}{m^*}$ can be obtained using Eq. (11) as follows [46]:

$$n^2 = \varepsilon_L - \left(\frac{e^2}{4\pi^2c^2\varepsilon_0}\right)\left(\frac{N}{m^*}\right)\lambda^2. \tag{11}$$

The values of ε_L and $\frac{N}{m^*}$ obtained are listed in Table 1, and an increase is observed in both ε_L and $\frac{N}{m^*}$ Higher Sm ratios suggest that the optical and electronic properties of the Zn_{100-x} Sm_x O thin films are more favorable for polarization and charge transport. This enhancement can lead to improved performance in optoelectronic applications.

The transport characteristics, grain and grain boundaries, and structure of the compounds can be ascertained using the dielectric loss (ε_2) and dielectric constant (ε_1). Moreover, a material's ability to retain electrical energy can be determined using the dielectric constant [47–52].

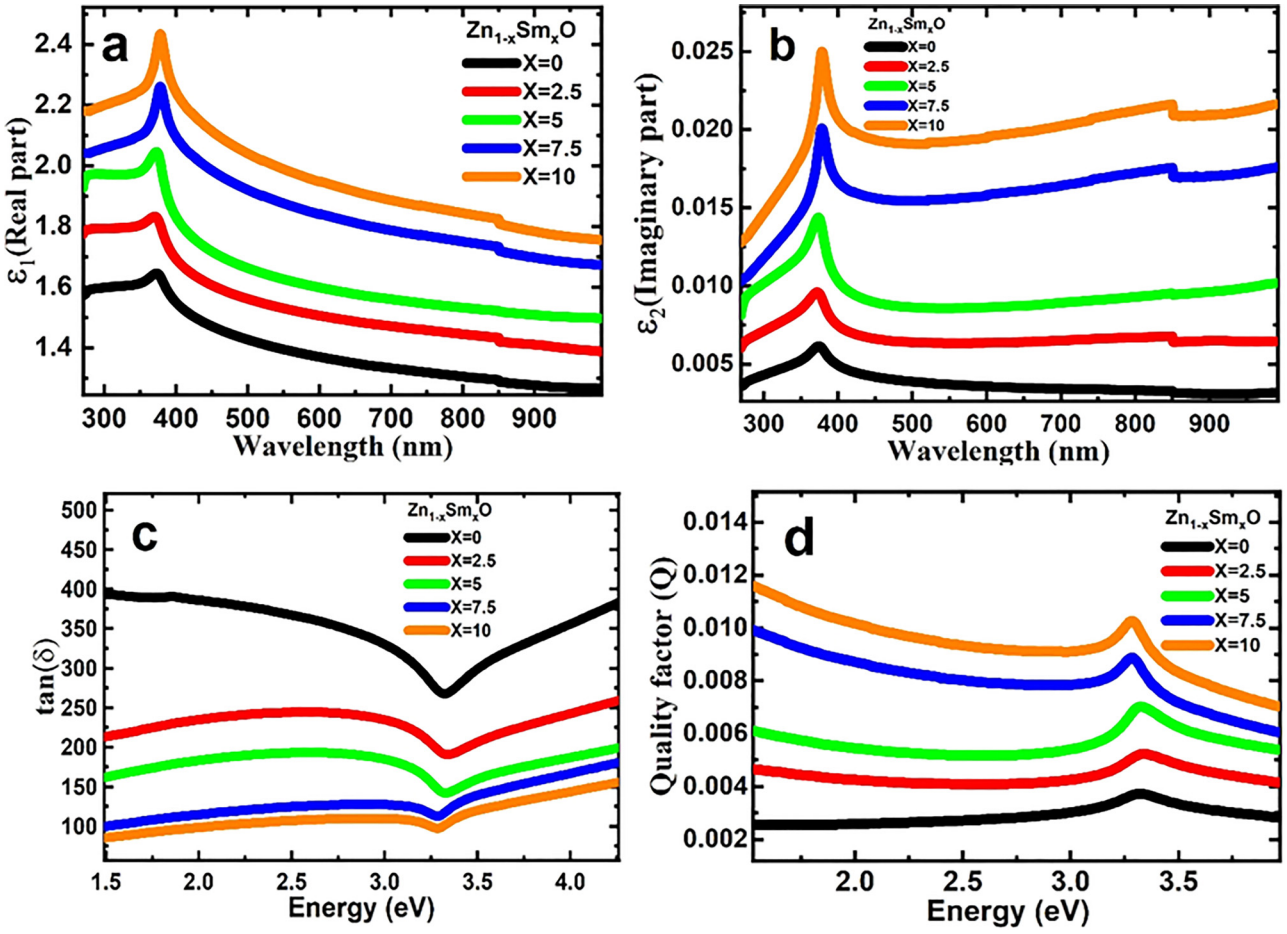

Figure 11: Plotting of the real (a) and imaginary (b) part of the dielectric constant *vs* wavelength, and dielectric loss tangent (c) and quality factor (d) *vs* *hv* $Zn_{100-x}Sm_xO$ thin films.

They also outline the properties of materials' responses to light and electric fields. While the actual part influences the refractive index and phase velocity of light in a medium, the imaginary part deals with absorption and shows how much light is absorbed by the substance. The following formulas are used to obtain the real and imaginary dielectric constants of the thin films [53]:

$$\varepsilon_1 = n^2 - k^2, \tag{12}$$

$$\varepsilon_2 = 2nk. \tag{13}$$

Figure 11a illustrates the wavelength dependence of ε_1 for the $Zn_{100-x}Sm_xO$ thin films. A clear trend of increasing ε_1 with higher Sm ratios (x) is observed across the entire wavelength range. This enhancement in ε_1 signifies an increased polarization capability within the material, suggesting that the incorporation of samarium introduces additional dipoles or enhances the existing electronic polarizability, leading to a stronger dielectric response. This observation directly correlates with the findings regarding the linear susceptibility (χ^1) and linear refractive index (n), where both were shown to increase with Sm doping. A higher ε_1 directly translates to a larger n, which is consistent with the enhanced linear optical response. The prominent peaks observed in ε_1 around 350–400 nm are indicative of resonant absorption phenomena occurring near the fundamental absorption edge, aligning well with the bandgap energies determined from the T_{auc} plot analysis.

Similarly, Figure 11b displays the wavelength dependence of ε_2, revealing an increase in its values with higher Sm concentrations. As ε_2 is directly proportional to the extinction coefficient (k) and, consequently, the absorption

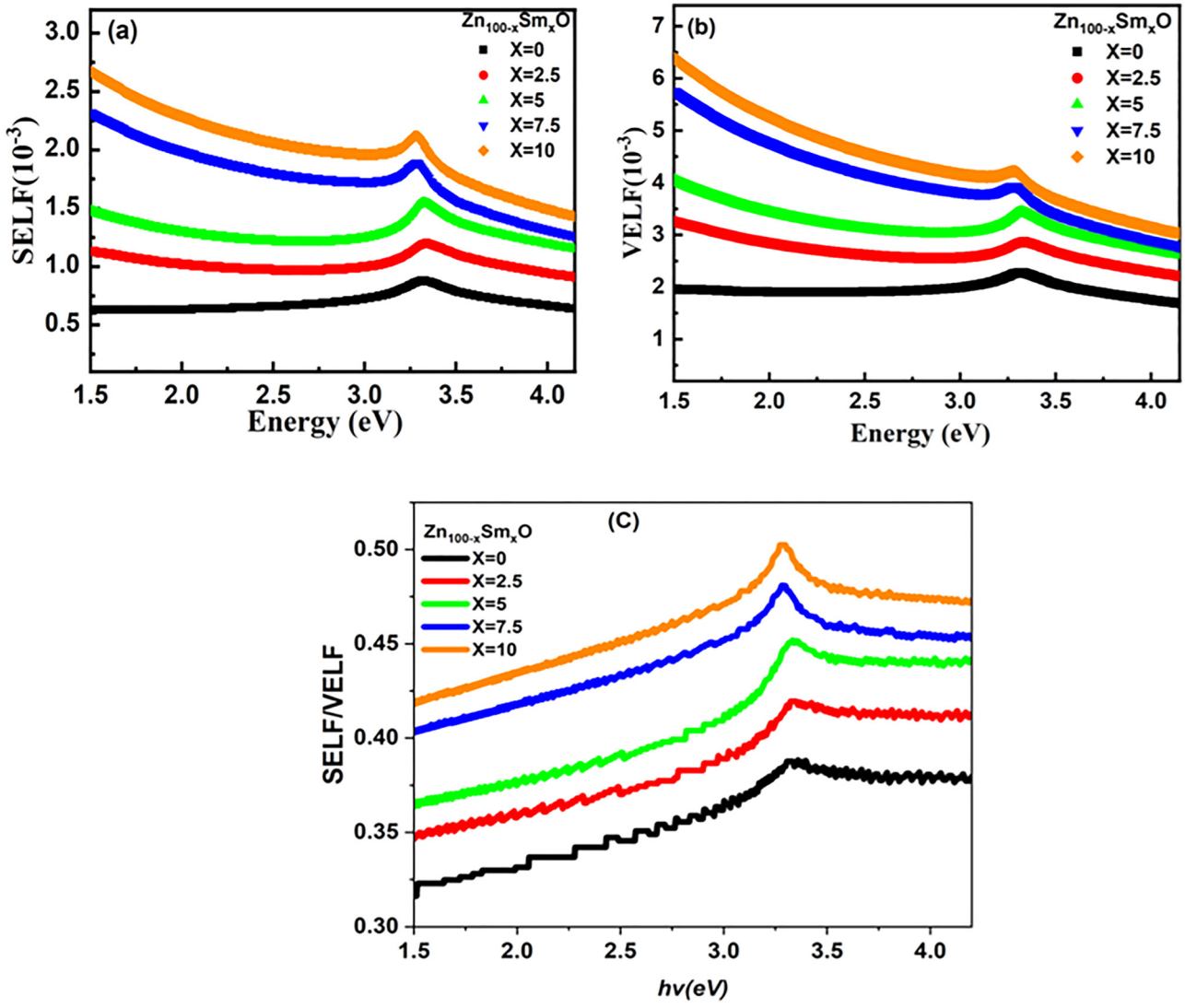

Figure 12: The change in (a) SELF, (b) VELF, and (c) SELF/VELF with hv for $Zn_{100-x}Sm_xO$ thin films.

coefficient (α), this trend is in excellent agreement with our earlier absorption coefficient spectra, which showed a significant increase in absorption with increasing Sm content. The increase in ε_2 suggests the existence of more mechanisms for energy dissipation within the material, likely due to enhanced inter-band transitions or defect-related absorption processes introduced or modified by Sm incorporation. The peaks in ε_2 also occur in the same energy range as those in ε_1, further confirming their association with the fundamental absorption edge and the onset of strong inter-band transitions.

Figure 11c presents the photon energy dependence of the dielectric loss tangent ($\tan(\delta) = \varepsilon_1/\varepsilon_2$) [38]. Interestingly, despite the increases in both ε_1 and ε_2, $\tan(\delta)$ is observed to decrease as the ratio of Sm increases. This reduction in $\tan(\delta)$ implies an improvement in the dielectric quality of the films. It suggests that while both the energy storage (polarization) and energy dissipation mechanisms are enhanced by Sm doping, the capacity for energy storage increases proportionally more than the energy dissipation. This phenomenon is attributed to the modified electronic energy levels resulting from Sm incorporation into the thin films. These modifications not only enhance the material's polarizability and absorption but also lead to a more efficient dielectric response, potentially by optimizing the balance between the energy storage and dissipation or by reducing certain loss pathways.

Two important parameters determine the thin film electron transition characterization: (the surface energy loss function (SELF) and volume energy loss function (VELF) [54–56]. SELF/VELF represents the ratio describing electron transitions in the examined thin film specialist and energies, which are low and high [56]. SELF and VELF of the current films can be computed by using the following equation [53] (Figure 12a and b):

$$\text{SELF} = \frac{\varepsilon_2}{(\varepsilon_1 + 1)^2 + \varepsilon_2^2}, \tag{14}$$

$$\text{VELF} = \frac{\varepsilon_2}{\varepsilon_1^2 + \varepsilon_2^2}. \tag{15}$$

From Figure 12, it is noticed that the SELF and VELF values increase as the Sm ratio increases. It is related to changes in the electron transition energy as Sm was incorporated into the thin films. Figure 12c shows the ratio of SELF/VELF *vs* the photon energy, and indicates that the addition of Sm to the thin films impacts the electron transition of the films.

An essential measure for understanding the electronic characteristics of thin films is the optical conductivity (σ_{Opt}), which is closely connected to the dielectric properties that describe how the materials interact with radiation. The following relation can be used to obtain σ_{Opt} [57,58]:

$$\sigma_{\text{Opt}} = \frac{\alpha n c}{4\pi}, \tag{16}$$

where the absorption coefficient, the refractive index, and the speed of light are denoted by α, n, and c, respectively. The correlation between σ_{Opt} of the $Zn_{100-x}Sm_xO$ thin film and the wavelength is shown in Figure 13a. As the Sm ratio increases, it is observed that σ_{Opt} increases as well; the maximum optical conductivity was achieved for the highest Sm ratio. This could be ascribed to the modifications made to the electrical structure of the thin films with the addition of Sm. The degree of polarization is closely correlated with the material's electric susceptibility for any

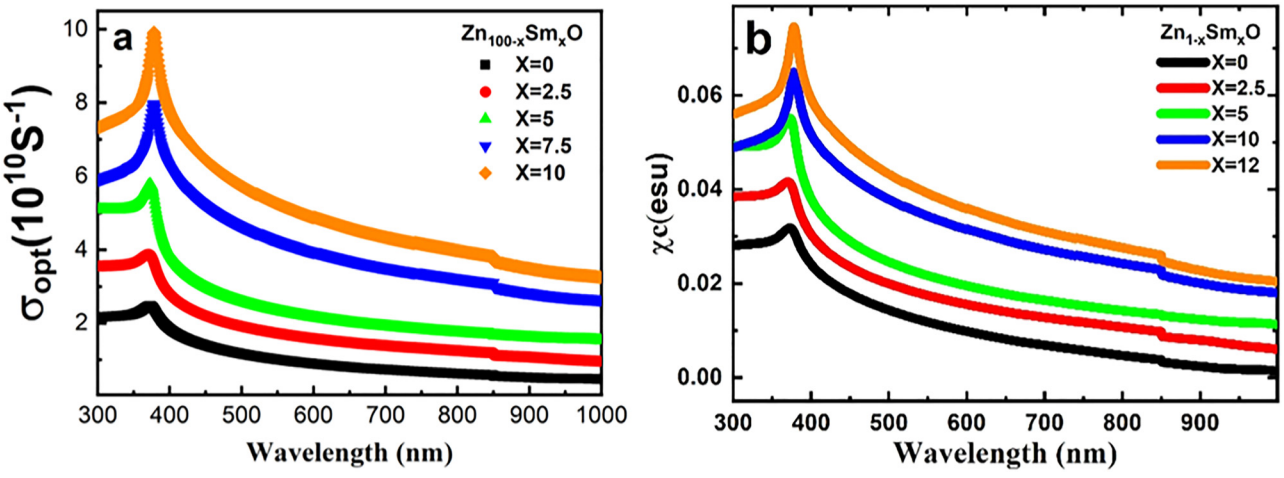

Figure 13: Plotting of (a) the optical conductivity and (b) the electrical susceptibility *vs* wavelength for $Zn_{100-x}Sm_xO$ thin films.

polarizable material. The electric sensitivity is a measure of how much the substance will polarize when exposed to an electric field. A material with a higher electric susceptibility can become more polarized when exposed to an electric field, which lowers the material's net electric field. The electric susceptibility (χ_c) can be found using the following expression [57]:

$$\chi_c = \frac{1}{4\pi}[n^2 - k^2 - n_0^2]. \tag{17}$$

The equation includes n, k, and n_0 parameters, which represent the thin film's refractive index, extinction coefficient, and the index of refraction for the surroundings, respectively. As illustrated in Figure 13b, the electric susceptibility χ_c increases proportionally with the Sm-to-Zn ratio in the film. This trend arises because Sm incorporation modifies the electronic band structure, altering the material's interaction with applied electric fields. Additionally, the disparity in polarizability between Sm and Zn ions enhances χ_c as the Sm content increases, as polarizability directly influences charge distribution under external fields.

The nonlinear refractive index (n_2) and the linear (χ^1) and nonlinear (χ^3) susceptibility for a material are given as follows [59]:

$$\chi^{(1)} = \frac{E_d/E_0}{4\pi}, \tag{18}$$

$$\chi^{(3)} = 6.82 \times 10^{-15} \times (E_d/E_0)^4 \ (e.\ s.\ u.), \tag{19}$$

$$n_2 = \frac{12\pi\chi^{(3)}}{n_0}. \tag{20}$$

Figure 14a–c displays the wavelength dependence of the nonlinear refractive index (n_2), linear susceptibility (χ^1), and nonlinear susceptibility (χ^3) for the $Zn_{100-x}Sm_xO$ thin films, respectively. The three parameters show the same pattern. As the ratio of Sm increases, it is generally seen that the values of χ^1, χ^3, and n_2 increase as well. This is also because of the altered polarizability and electronic structure that result from the addition of Sn to the thin

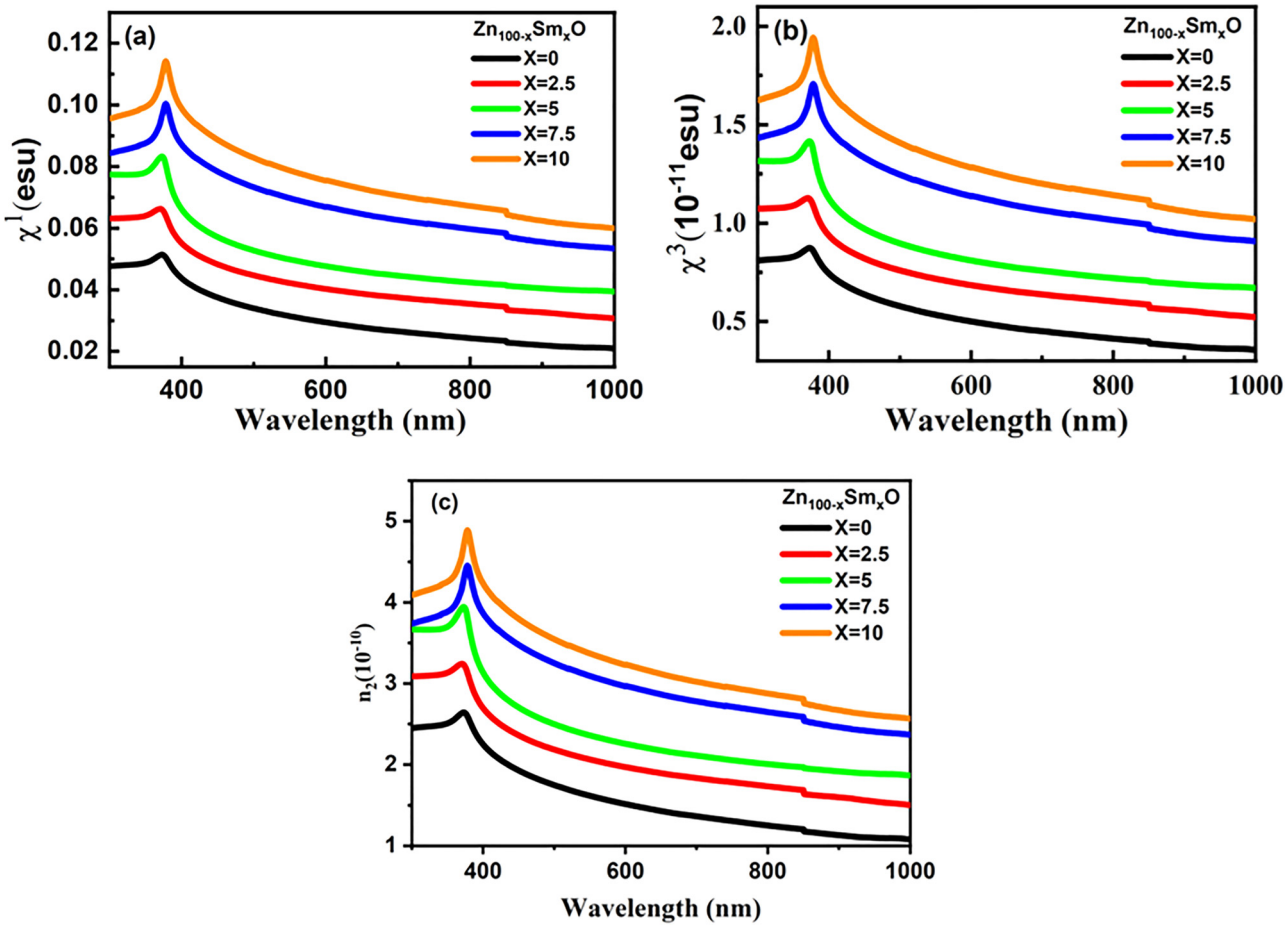

Figure 14: The difference of (a) the linear, (b) the non-linear susceptibility, and (c) non-linear refractive index with λ for $Zn_{100-x}Sm_xO$ thin films.

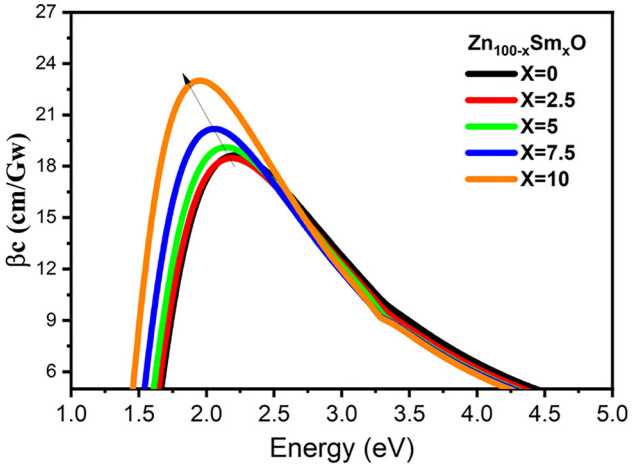

Figure 15: Non-linear absorption coefficient (β) $Zn_{100-x}Sm_xO$ thin films.

films [60]. The modified optical characteristics of the $Zn_{100-x}Sm_xO$ thin films are advantageous for a variety of uses. Controlling nonlinear characteristics makes frequency conversion and optical limiting easier. Furthermore, developing advanced materials for photonic and optoelectronic devices is facilitated by understanding these changes [61].

Figure 15 exhibits the variation in the nonlinear absorption coefficient (βc) and the energy for the $Zn_{100-x}Sm_xO$ thin films. The maximum value of βc is shifted towards a lower energy photon as the ratio of Sm increases. Doping Sm can establish additional energy levels inside the band gap. Because electrons can be excited from these confined states into the conduction band, these mid-gap states can help absorb lower-energy photons. Since additional photon energies are now resonant with these states, the nonlinear absorption coefficient increases at lower energies. Two-photon absorption and saturable absorption are two of the optical processes that affect the nonlinear absorption coefficient. The density of states varies with increasing Sm ratio, changing the way these processes occur. Increased nonlinear absorption at lower energies could result from stronger interactions between photons and bound electron–hole pairs or exciton states.

5 Conclusion

The investigation of $Zn_{100-x}Sm_xO$ thin films synthesized *via* the sol–gel combustion method reveals significant enhancements in structural, optical, and electronic properties with increasing Sm doping. XRD and SEM analyses confirm a reduction in the grain size and lattice parameters, inducing structural strain that correlates with improved surface densification and reduced porosity. Optical studies demonstrate increased absorbance, a narrowed bandgap (from 3.12 to 2.77 eV), and elevated refractive index and dielectric constants, attributed to Sm-induced electronic states and polarizability. The increase in SELF, VELF, optical conductivity, and nonlinear optical parameters (n_2, χ^1, and χ^3) highlights enhanced light–matter interactions, beneficial for optoelectronic and photocatalytic applications. These findings underscore the potential of Sm-doped ZnO nanocomposites for advanced optical devices, aligning with sustainable material development trends, and pave the way for further optimization in energy harvesting and environmental technologies.

Acknowledgments: The authors express their gratitude to Princess Nourah bint Abdulrahman University Researchers Supporting Project number (PNURSP2025R223), Princess Nourah bint Abdulrahman University, Riyadh, Saudi Arabia.

Funding information: The authors express their gratitude to Princess Nourah bint Abdulrahman University Researchers Supporting Project number (PNURSP2025R223), Princess Nourah bint Abdulrahman University, Riyadh, Saudi Arabia.

Author contributions: Amira Ben Gouider Trabelsi and Mahmoud M. Abou Halaka – methodology and writing; Fatemah H. Alkallas and Abdelaziz M. Aboraia – writing, supervision, and project management; and Wael M. Mohammed and Mohamed S. I. Koubisy – supervision and revising the data. All authors have accepted responsibility for the entire content of this manuscript and approved its submission.

Conflict of interest: The authors state no conflict of interest.

Data availability statement: All data generated or analyzed during this study are included in this published article.

References

[1] Dhirendra KSh, Sweta Sh, Kapil KSh, Vipin K. A review on ZnO: Fundamental properties and applications. Mater Today: Proc. 2022;49:3028–35.

[2] Chitra M, Mangamma G, Uthayarani K, Neelakandeswari N, Girija EK. Band gap engineering in ZnO based nanocomposites. Phys E. 2020;119:113969.

[3] Dejene F, Ali A, Swart H, Botha R, Roro K, Coetsee L, et al. Optical properties of ZnO nanoparticles synthesized by varying the sodium

hydroxide to zinc acetate molar ratios using a Sol-Gel process Cent. Eur J Phys. 2011;9(5):1321–6.
[4] Zhou J, Xu NS, Wang ZL. Dissolving behavior and stability of ZnO wires in biofluids: A study on biodegradability and biocompatibility of ZnO nanostructures. Adv Mater. 2006;18:2432–5.
[5] Badreddine K, Kazah I, Rekaby M, Awad R. Structural, morphological, optical, and room temperature magnetic characterization on pure and Sm-doped ZnO nanoparticles. J Nanomater. 2018;18:796195.
[6] İpek Y, Ayhan NaKa. Rare earth element doped ZnO thin films and applications. Int J Pure Appl Sci. 2021;7(2):305–13.
[7] Chawla S, Saroha M, Kotnala RK. White light emitting magnetic ZnO: Sm nanoparticles prepared by inclusive co-precipitation synthesis. Electron Mater Lett. 2014;10:73–80.
[8] Lang J, Zhang Q, Han Q, Fang Y, Wang J, Li X, et al. The study of structural and optical properties of (Eu, La, Sm) codoped ZnO nanoparticles via a chemical route. Mater Chem Phys. 2017;194:29–36.
[9] Sin JC, Lam SM, Lee KT, Mohamed AR. Preparation and photocatalytic properties of visible light-driven samarium-doped ZnO nanorods. Ceram Int. 2013;39:5833–43.
[10] Singh J, Singh GP, Kumar S, Jain RK, Gasso S, Singh B, et al. Probing structural, optical and magnetic properties of Sm-doped ZnO nanomaterials via experimental and DFT approach: Enhanced photocatalytic degradation and antibacterial performance. Colloids Surf A: Physicochem Eng Asp. 2023;668:131470.
[11] Malhotra JS, Singh AK, Khosla R, Sharma SK, Sharma G, Kumar S. Investigations on structural, optical and magnetic properties of Fe and Dy co-doped ZnO nanoparticles. J Mater Sci: Mater Electron. 2018;29:3850–5.
[12] Kaneva N, Bojinova A, Papazova K, Dimitrov D. Photocatalytic purification of dye contaminated sea water by lanthanide (La^{3+}, Ce^{3+}, Eu^{3+}) modified ZnO. Catal Today. 2015;252:113–9.
[13] Akhtar J, Tahir MB, Sagir M, Bamufleh HS. Improved photocatalytic performance of Gd and Nd co-doped ZnO nanorods for the degradation of methylene blue. Ceram Int. 2020;46:11955–61.
[14] Ayon SA, Jamal M, Muktadir Billah Md, Neaz S. Augmentation of magnetic properties and antimicrobial activities of band gap modified Ho^{3+} and Sm^{3+} doped ZnO nanoparticles: A comparative experimental study. J Alloy Compd. 2022;897:163179.
[15] Alam U, Khan A, Ali D, Bahnemann D, Muneer M. Comparative photocatalytic activity of sol–gel derived rare earth metal (La, Nd, Sm and Dy)-doped ZnO photocatalysts for degradation of dyes. RSC Adv. 2018;8:17582–94.
[16] Ahmed MAM, Mwankemwa BS, Carleschi E, Doyle BP, Meyer WE, Nel JM. Effect of Sm doping ZnO nanorods on structural optical and electrical properties of Schottky diodes prepared by chemical bath deposition. Mater Sci Semicond Process. 2018;79:53–60.
[17] Tsuji T, Terai Y, Bin Kamarudin MH, Kawabata M, Fujiwara Y. Photoluminescence properties of Sm-doped ZnO grown by sputtering-assisted metalorganic chemical vapor deposition. J Non Cryst Solids. 2012;358:2443–5.
[18] Thool GS, Arunakumari M, Singh AK, Singh SP. Shape tunable synthesis of Eu- and Sm-doped ZnO microstructures: A morphological evaluation. Bull Mater Sci. 2015;38:1519–25.
[19] Koubisy MSI, Mohammed W, Alkallas FH, Trabelsi ABG, Alraddadi Sh, Aboraia AM. Effect of Sn on the structural, morphological and optical properties of $LiCoPO_4$. Opt Mater. 2025;163:116977.
[20] Sakai N, Ebina Y, Takada K, Sasaki T. Electronic band structure of titania semiconductor nanosheets revealed by electrochemical and photoelectrochemical studies. J Am Chem Soc. 2004;126(18):5851–8.
[21] Wang Y, Dong Y, Zhou L, Kang J, Wang N, He J. 2D Nb_2CT_x MXene/MoS_2 heterostructure construction for nonlinear optical absorption modulation. Opto-Electron Adv. 2023;6(10):220162.
[22] Bafekry A, Nguyen C, Obeid MM, Ghergherehchi M. Modulating the electro-optical properties of doped C_3N monolayers and graphene bilayers via mechanical strain and pressure. N J Chem. 2020;44(36):15785–92.
[23] Amini A, Porciatti E, Minotto A, Moranchel ÁT, Sassella A, Canziani R, et al. Exploring optical properties and radiation transfer in a mixed culture of purple phototrophic bacteria grown in a flat-plate photobioreactor via combined experimental and modelling approach. J Environ Chem Eng. 2025;13:115425.
[24] Alasmari A, Hassan AM, Aboraia AM, Mahmoud AE. Influence of oxygen flow rate on phase transformation, electronic properties, and spectral-coefficient characteristic of V_xO_y thin films deposited via reactive magnetron sputtering. Phys B: Condens Matter. 2025;700:416892.
[25] Aboraia AM, El Refaay DE, Henaish A, Elnage H, Alraddadi S, Hassan AM, et al. Turning the structural as well as optical characteristics of ZiF-8 thin coatings through inclusion of reduced graphene oxide: a comparative study. Opt Quantum Electron. 2024;57(1):38.
[26] Davis EA, Mott NF. Conduction in non-crystalline systems V. Conductivity, optical absorption and photoconductivity in amorphous semiconductors. Philos Mag. 1970;22:0903–22.
[27] Diab F, Ali IA, Hassan AM. Effect of successive plasma shots on the dielectric constant of the CdS:Mn thin films exposed to the helium electron beam of plasma focus device. Sens Actuat A: Phys. 2021;329:112819.
[28] Choudhury B, Choudhury A. Oxygen defect dependent variation of band gap, Urbach energy and luminescence property of anatase, anatase–rutile mixed phase and of rutile phases of TiO_2 nanoparticles. Phys E: Low-Dimens Syst Nanostruct. 2014;56:364–71.
[29] Brahimi R, Dib K, Trari M, Bessekhouad Y. Effect of S-doping toward the optical properties of WO_3 nanoparticles. Mater Chem Phys. 2019;223:398–403.
[30] Diab F, Hassan AM. Influence of a plasma focus device on the structural and optical properties of highly conductive AZO thin films. Materials Today. Communications. 2024;40:109856.
[31] Tauc J, Menth A. States in the gap. J Non-Cryst Solids. 1972;8:569–85.
[32] Koubisy MSI, Zatsepin AF, Biryukov DY, Zatsepin DA, Shtang TV, Gavrilov NV. Ion-beam induced quasi-dynamic continual disorder in Bi-implanted Hongan silica glass. J Non Cryst Solids. 2021;563:120818.
[33] Aïnouche L, Hamadou L, Kadri A, Benbrahim N, Bradai D. Ti^{3+} states induced band gap reduction and enhanced visible light absorption of TiO_2 nanotube arrays: Effect of the surface solid fraction factor. Sol Energy Mater Sol Cell. 2016;151:179–90.
[34] Zatsepin AF, Kuznetsova YA, Shtang TV, Mikhaylov AN, Koubisy MSI. New optical oxygen-deficient centers in 80 keV Re-implanted amorphous silica. J Non Cryst Solids. 2020;529:119775.
[35] Chomicki D, Kharchenko O, Skowronski L, Kowalonek J, Kozanecka-Szmigiel A, Szmigiel D, et al. Physico-chemical and light-induced properties of quinoline azo-dyes polymers. Int J Mol Sci. 2020;21(16):5755.

[36] Aboraia AM, Yahia IS, Saad M, Alsulaim G, Alnahdi KM, Alsharif SA, et al. Exploration of the structural rGO thin films and their optical characteristics for optoelectronic device applications. J Opt. 2024;1–10.
[37] Zhukovsky M, Koubisy MSI, Zakaly HMH, Ali AS, Issa SAM, Tekin HO. Dielectric, structural, optical and radiation shielding properties of newly synthesized $CaO–SiO_2–Na_2O–Al_2O_3$ glasses: Experimental and theoretical investigations on impact of Tungsten (III) oxide. Appl Phys A. 2022;128(3):205.
[38] Wemple SH, DiDomenico M Jr. Behavior of the electronic dielectric constant in covalent and ionic materials. Phys Rev B. 1971;3(4):1338.
[39] Sahoo D, Priyadarshini P, Dandela R, Alagarasan D, Ganesan R, Varadharajaperumal S, et al. In situ laser irradiation: the kinetics of the changes in the nonlinear/linear optical parameters of As_{50} Se_{40} Sb_{10} thin films for photonic applications. RSC Adv. 2021;11:16015–25.
[40] Hassan AM, Alyousef HA, Zakaly HMH. Optimizing the structure and optoelectronic properties of cuprite thin films via a plasma focus device as a solar cell absorber layer. CrystEngComm. 2024;26:1590–606.
[41] Mohamed HFM, Abdel-Hady EE, Mohammed WM. Investigation of transport mechanism and nanostructure of nylon-6,6/PVA blend polymers. Polymers. 2023;15:107.
[42] Mohammed WM, Awad S, Abdel-Hady EE, Mohamed HFM, Elsharkawy YS, Elsharkawy MRM. Nanostructure analysis and dielectric properties of PVA/sPTA proton exchange membrane for fuel cell applications: Positron lifetime study. Radiat Phys Chem. 2023;208:110942.
[43] Alyousef HA, Hassan AM, Zakaly HMH. Reactive magnetron sputtered AlN thin films: structural, linear and nonlinear optical characteristics. J Mater Sci: Mater Electron. 2023;34:1088.
[44] Rashad M, Darwish A. Blue shift of band gap for vanadyl 2,3-naphthalocyanine (VONc) thin films monitored at thermal effects. Mater Res Express. 2018;5(2):026402.
[45] Elsharkawy MR, Mohammed WM. Effect of the electric field on the free volume investigated from positron annihilation lifetime and dielectric properties of sulfonated PVC/PMMA. Polym Adv Technol. 2024;35(7):6519.
[46] Zatsepin A, Kuznetsova Yu, Zatsepin DA, Boukhvalov D, Nikolay G, Koubisy M. Electronic Structure and Optical Absorption in Gd-Implanted Silica Glasses. Phys Status Solidi (A) Appl Mater Sci. 2019;216(3):1800522.
[47] Mohamed HF, Taha HG, Mohammed WM, Abdel-Hady EE, Awad S. Study of mechanical and electrical properties through positron annihilation spectroscopy for ethylene-propylene-diene rubber biocomposites with treated wheat husk fibers. Sci Rep. 2024;14(1):24302.
[48] Mohammed WM, El-Desoky MM, Abdllah N, Mohamed HF, Abdel-Hady EE, El Refaay DE. Relationship between structural, electrical properties and positron annihilation parameters of $V_2O_5–Cu_2O–P_2O_5$ glasses. Phys B: Condens Matter. 2024;694:416459.
[49] Mohamed HF, Abdel-Hady EE, Hassanien MH, Mohammed WM. Investigation of the impact of an electric field on polymer electrolyte membranes for fuel cell applications. Physics. 2024;6(4):1345–65.
[50] Aboraia AM, El Refaay DE, Henaish A, Elnage H, Alraddadi S, Hassan AM, et al. Tuning the structural as well as optical characteristics of ZiF-8 thin coatings through inclusion of reduced graphene oxide: a comparative study. Opt Quantum Electron. 2024;57(1):38.
[51] Mohammed WM, Saad HM, Aboraia AM, Elella MHA, Abdelkhalik A, Goda ES. 10 - Rheological behavior of PVC-based blends, IPNs, and gels. In Poly(vinyl chloride)-based blends, interpenetrating polymer networks (IPNs), and gels. Elsevier; 2024. p. 255–80.
[52] Ravi A, Samuel J, Sahaya Jude Dhas S, Usharani S, Simon T, Senthil Kumar D, et al. Structural, morphological, optical and antibacterial performances of rare earth (Sm)-doped ZnO nanorods. J Rare Earths. 2024;42:2119–27.
[53] Ali AI, Son JY, Ammar AH, Abdel Moez A, Kim YS. Optical and dielectric results of $Y_{0.225}Sr_{0.775}CoO_{3\pm\delta}$ thin films studied by spectroscopic ellipsometry technique. Results Phys. 2013;3:167–72.
[54] Giri S, Priyadarshini P, Alagarasan D, Ganesan R, Naik R. Annealing-induced phase transformation in $In_{10}Se_{70}Te_{20}$ thin films and its structural, optical and morphological changes for optoelectronic applications. RSC Adv. 2023;13(36):24955–72.
[55] Tholkappiyan R, Hamed F, Vishista K. Effect of annealing conditions on the struct-optical properties of $ZnFe_{1.96}La_{0.04}O_4$ nanoparticles. Adv Mater Lett. 2016;7(12):971–8.
[56] El-naggar AM, Heiba ZK, Mohamed MB, Kamal AM, Lakshminarayana G. PVA/PVP/PEG polymeric blend loaded with nano-$Zn_{0.75-x}Fe_x$ $Cd_{0.25}S$: effect of iron concentration on the optical characteristics. Appl Phys A. 2022;128(3):220.
[57] Khenata R, Bouhemadou A, Sahnoun M, Reshak AH, Baltache H, Rabah M. Elastic, electronic and optical properties of ZnS, ZnSe and ZnTe under pressure. Comput Mater Sci. 2006;38(1):29–38.
[58] Boyd R. Nonlinear optics. Vol. 19922. San Diego, Calif: Academic; 2008. p. 39.
[59] Alghamdi HM, Rajeh A. Integrating the structural, optical, magnetic, electrical, and dielectric properties of PAM/PEO/$NiCo_2O_4$ nanocomposites for opto-magnetic and energy storage applications. Ceram Int. 2025;51:18045–55.
[60] Alqarni MA, Rajeh A. Optimizing the structural, optical, dielectric, and electrical properties of polyvinyl alcohol/polyvinyl pyrrolidone/zinc manganite nanocomposites for optical and energy storage applications. Results Phys. 2024;67:108045.
[61] Elamin NY, Modwi A, Abd El-Fattah W, Rajeh A. Synthesis and structural of Fe_3O_4 magnetic nanoparticles and its effect on the structural optical, and magnetic properties of novel Poly (methyl methacrylate)/Polyaniline composite for electromagnetic and optical applications. Opt Mater. 2023;135:113323.